

SubT-MRS: A Subterranean, Multi-Robot, Multi-Spectral and Multi-Degraded Dataset for Robust SLAM

Shibo Zhao^{*1} Tianhao Wu¹ Yuanjun Gao¹ Damanpreet Singh¹ Rushan Jiang¹
 Haoxiang Sun¹ Jay Karhade¹ Ian Higgins¹ Warren Whittaker¹ Lucas Nogueira¹
 Tingting Da¹ Mansi Sarawata¹ Can Xu¹ Jiahe Xu¹ He Yao¹
 Sourojit Saha¹ Yuheng Qiu¹ Wenshan Wang¹ Chen Wang¹ Sebastian Scherer¹

¹Carnegie Mellon University

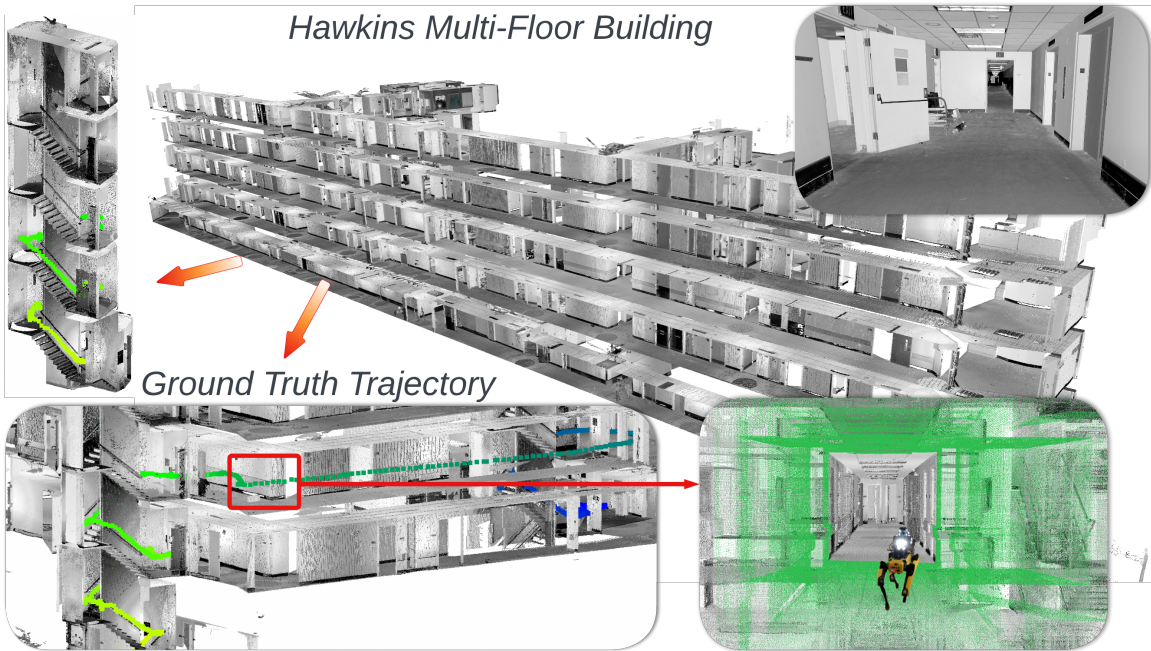


Figure 1: Ground truth dense, high-quality reconstruction map and Ground truth trajectory generation

Abstract

In recent years, significant progress has been made in the field of simultaneous localization and mapping (SLAM) research. However, current state-of-the-art solutions still struggle with limited accuracy and robustness in real-world applications. One major reason is the lack of datasets that fully capture the conditions faced by robots in the wild. To address this problem, we present SubT-MRS, an extremely challenging real-world dataset designed to push the limits of SLAM and perception algorithms.

SubT-MRS is a multi-modal, multi-robot dataset col-

lected mainly from subterranean environments having multi-degraded conditions including structureless corridors, varying lighting conditions, and perceptual obscurants such as smoke and dust. Furthermore, the dataset packages information from a diverse range of time-synchronized sensors, including LiDAR, visual cameras, thermal cameras, and IMUs captured using varied vehicular motions like aerial, legged, and wheeled, to support research in sensor fusion, which is essential for achieving accurate and robust robotic perception in complex environments. To evaluate the accuracy of SLAM systems, we also provide a dense 3D model with sub-centimeter-level accu-

racy, as well as accurate 6DoF ground truth. Our benchmarking approach includes several state-of-the-art methods to demonstrate the challenges our datasets introduce, particularly in the case of multi-degraded environments.

1. Introduction

Robustness is essential for SLAM systems to ensure accurate and reliable estimates despite the noise, errors, uncertainties, and unexpected events. This is especially critical in complex field robotic applications, where SLAM provides precise maps and localization for tasks such as collaborative exploration, multi-robot search and rescue, and autonomous off-road driving.

Despite significant advancements in state-of-the-art SLAM algorithms such as VINS-MONO, LIO-SAM, and ORB-SLAM3[19, 24, 3], they struggle to perform well in real-time online missions due to the lack of good training datasets. When evaluated on datasets that do not capture real-life SLAM challenges, algorithms become biased towards underchallenging environments, resulting in poor performance in real-life scenarios. Therefore, it is crucial to create a dataset that can capture and emulate the real-life challenges faced by SLAM algorithms, such as sensor degradation, perceptual obscurants, and weather changes.

In recent years, several datasets have been developed to achieve this. For example, handheld datasets such as [12, 21, 17, 22, 30] present indoor-outdoor scenarios with illumination changes, but are limited to a single kinematic profile, walking, and do not incorporate challenges of high-speed car-like motion. On the other hand, datasets like EuRoC-MAV[2] and UZH-FPV[6] provide visual-inertial datasets for drones with high-speed, holonomic motion, but they lack multiple sensors and are only suitable for well-lit areas. While KITTI, TartanAir, and Hilti Challenge[11, 25, 12] include more than two sensors and sensor-degraded scenarios, they lack multiple kinematic profiles. Additionally, most leading datasets only contain single-robot datasets and do not support research in multi-robot SLAM. A tabular comparison for these datasets can be seen in Table 1.

To address these limitations, we present our dataset, **Subterranean**, **Multi-Robot**, **Multi-Spectral-Inertial**, and **Multi-Degraded (SubT-MRS)**, which has the following characteristics:

- **Multiple Modalities:** Our dataset packages hardware time-synchronized data from 4 RGB cameras, 1 LiDAR, 1 IMU, and 1 thermal camera.
- **Diverse Scenarios:** Our dataset has been collected at multiple locations with varying environmental setups, such as indoors, outdoors, mixed indoor-outdoor, underground, off-road, buildings, etc.
- **Multi-Degraded:** Owing to the fact that our dataset has 4 different modalities and multiple environmen-

tal scenarios, we have multiple permutations of sensor degradation, ranging from single sensor failure to multi-sensor failure induced by perceptual obscurants like fog, snow, smoke, illumination changes, etc, as can be seen in Figure 2.

- **Heterogeneous Kinematic Profiles:** Our dataset is the first dataset that includes time-synchronized sensor data from multiple holonomic and non-holonomic vehicles having different speed ranges. We have collected data using multiple RC cars, legged robot, drones, and handheld also.
- **Multi-Robot Data:** Our dataset is the first one to provide time-synchronized multi-robot data using multiple vehicles with heterogeneous kinematic profiles.

Based on the listed features, our dataset represents a significant advancement over existing SLAM datasets, as it encompasses a range of sensor modalities, kinematic profiles, and sensor degradations. A key feature of our dataset is the availability of data for multiple kinematic profiles within a single scene, including diverse weather conditions. This breadth of scenarios allows for close emulation of real-world conditions and provides a formidable challenge for any SLAM algorithm.

Here on, research work related to the dataset is presented in Section 2, followed by details about the hardware aspect of the dataset in Section 3, including discussions on the sensor payload, calibrations, and time synchronizations. Subsequently, Section 4 discusses the dataset’s features, while Section 5 details the procedure for generating ground truth maps and trajectories. Finally, Section 6 evaluates various SLAM algorithms on our dataset and provides a conclusion by discussing the results and findings.

2. Related Work

Over the past decade, numerous SLAM datasets have emerged, aiming to replicate various real-life scenarios faced by SLAM algorithms such as sensor degradation, vehicular motion, and weather changes. Most of these datasets focus on visual-inertial data, reflecting the SLAM community’s interest in visual-inertial SLAM due to the ease of setting up a visual-inertial sensing system. This trend is evident in state-of-the-art SLAM algorithms such as VINS-MONO, ORB-SLAM3, and LIO-SAM[19, 3, 24].

The TUM-VI dataset[22] is a popular indoor-outdoor visual-inertial dataset, collected on a custom sensor deck made of aluminum bars. It is a challenging dataset due to the presence of illumination changes in the indoor-outdoor transitions but lacks any high-speed motions. The UMA-VI dataset[30] is also another handheld indoor-outdoor visual-inertial dataset collected in low-textured and dynamic illuminated environments. The EuRoC MAV dataset[2] provides indoor SLAM data onboard a drone. The motion blur induced by the fast holonomic motion of the drone provides

Dataset	Multi-Spectrum				Multi-Degradation					Multi-Robot			
	Camera	IMU	Lidar	Thermal	Illumination	Snow Smoke	Structureless	Subt	Offroad	Vehicle	Drone	Legged	Handhold
EuRoC MAV [2]	✓	✓	✗	✓	✓	✗	✗	✗	✗	✗	✓	✗	✗
PennCOSYVIO [17]	✓	✓	✗	✗	✗	✗	✗	✗	✗	✗	✗	✗	✓
TUM VIO [22]	✓	✓	✗	✗	✗	✗	✗	✗	✗	✗	✗	✗	✓
UZH-FPV [6]	✓	✓	✗	✗	✗	✗	✗	✗	✓	✗	✓	✗	✗
KITTI [10]	✓	✓	✓	✗	✗	✗	✗	✗	✗	✓	✗	✗	✗
Virtual KITTI [9]	✓	✓	✗	✓	✗	✓	✗	✗	✗	✓	✗	✗	✗
College Dataset [28]	✓	✓	✓	✗	✗	✗	✗	✗	✗	✗	✗	✗	✓
RobotCar [16]	✓	✓	✓	✗	✓	✗	✓	✗	✗	✓	✗	✗	✗
UMA VI [30]	✓	✓	✗	✗	✓	✗	✓	✗	✗	✗	✗	✗	✓
UMich [4]	✓	✓	✓	✗	✓	✗	✗	✗	✗	✓	✗	✗	✓
Hilti SLAM [12]	✓	✓	✓	✗	✓	✗	✓	✗	✗	✗	✓	✗	✓
TartanAir [25]	✓	✓	✓	✗	✓	✓	✓	✗	✓	-	-	-	-
OURS	✓	✓	✓	✓	✓	✓	✓	✓	✓	✓	✓	✓	✓

Table 1: Comparison of SLAM datasets on multi-sensors, multi robots, and multi degradation.

a good challenge for SLAM algorithms. This dataset has been appreciated a lot by the SLAM community but lacks outdoor data. UZH-FPV drone racing dataset[6] incorporates the benefits of both TUM-VI and EuRoC by providing an indoor-outdoor drone dataset with aggressive motions. The Rosario dataset[18] is an example of visual-inertial data in non-holonomic motion as it records data onboard a wheeled robot but is only limited to agricultural fields.

SLAM algorithms relying merely on visual and inertial data tend to fail in environments with low visual texture, which is why many recent SLAM datasets include data from multiple sensing modalities. The KITTI dataset[10] provides extensive autonomous driving data in the form of outdoor LiDAR-visual-inertial data collected onboard a car along with GPS-based ground truth trajectory, making it the most popular benchmark in SLAM. However, it is unable to be extended to indoor SLAM challenges and does not have any fast motion, sensor degradation and challenging environment. The Hilti SLAM dataset[12] attempts to resolve this by including indoor-outdoor LiDAR-visual-inertial datasets captured on their custom-built sensor stick and gives a good challenge due to the presence of dynamic illumination and featureless spaces but the difficulty plateaus due to the absence of fast motion or additional kinematic profiles and absence of perceptual obscurants. Tartan Air[25] also provides abundant LiDAR-visual-inertial-stereo dataset but is far from the real-life SLAM challenges as the data is simulation-based and the motion kinematic profile is undefined.

We can see that all these state-of-the-art benchmarks for SLAM have saturated due to one or more of the following reasons:

- Lack of enough sensor degradation caused by perceptual obscurants like smoke, fog, and structureless environments.
- Lack of multiple motion kinematic profiles. Having different motion patterns induces different motional uncertainties and makes the data more challenging

- Lack of fast motion. Fast motion induces disruptions in sensory data, like skew and blur, which accounts for additional challenge

Our dataset is able to tackle these issues by having multiple sensors, diverse kinematic profiles, perceptual obscurants, and diverse environment and weather conditions.

There are only two peer-reviewed multi-robot SLAM (MR-SLAM) datasets available, both collected in controlled environments, limiting their ability to emulate real-life SLAM challenges. The UTIAS MR-CLAM dataset[14] used five identical slow-moving ground vehicles with monocular camera data, while the AirMuseum dataset[7] used three ground vehicles and a drone with stereo visual-inertial data. Although the AirMuseum dataset added a holonomic robot and was collected in a larger area, both datasets lack diversity in vehicular motion kinematics and fail to fully represent real-life SLAM challenges. Our dataset presents a significant improvement over these because of a bigger sensor stack per robot of LiDAR-visual-thermal-inertial data and diverse kinematic profiles with RC cars, legged robots, and drones.

3. Hardware

3.1. Sensor Payload

The sensor payload used for our dataset collection can be seen in Figure 3. This payload was designed by the Explorer team during the DARPA Subterranean Challenge and has been assembled rigidly with the purpose of protecting the sensors from external impacts and preventing any internal vibrations. Our sensor payload is equipped with 4 Leopard Imaging RGB monocular cameras, 1 Velodyne puck, 1 Epson M-G365 IMU, and 1 FLIR Boson thermal camera. The payload has an NVIDIA Jetson AGX Xavier as its onboard computer. The specifics for these components can be seen in Table 2.



Figure 2: SubT-MRS datasets were collected in various perceptually-degraded environments over different seasons. The scenarios include poor illumination, darkness, and water puddles, in which visual-based sensor fusion methods become unreliable. There are also geometrically degraded environments such as long featureless corridors and steep multi-floors which makes the lidar-based system prone to drift. Also, it includes airborne obscurant conditions such as dust, fog, snow, and smoke in challenging scenes including caves, deserts, long tunnels, and off-road environments.

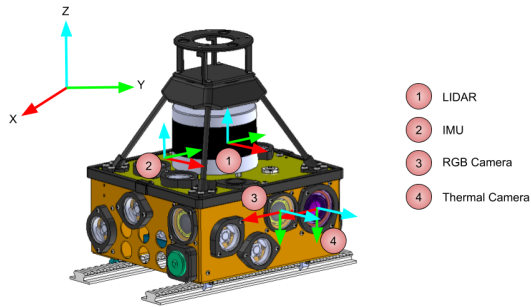


Figure 3: CAD model of the Payload.

Component	Type	Rate	Characteristics
Lidar	Velodyne VLP-16	10Hz	16 channels, 100m range
IMU	Epson M-G365	200Hz	Time Synchronization center
RGB Camera	LI-Xavier-Kit	24Hz	686×816 pixels
Thermal Camera	FLIR Boson	60Hz	512×640 pixels
Computer	Nvidia Jetson AGX Xavier	-	32GB RAM, 8 CPU cores

Table 2: Overview of sensors on the payload

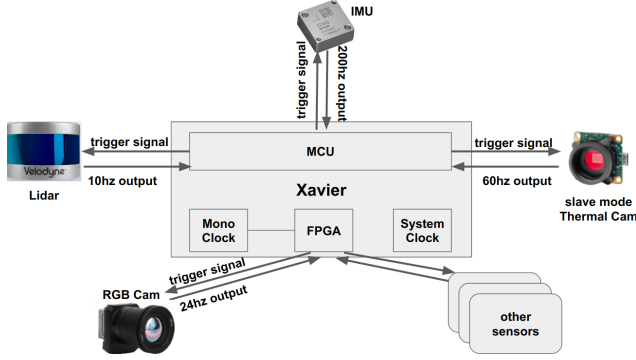


Figure 4: Sensor hardware time synchronization paradigm

3.2. Time Synchronization of Sensors

Time synchronization plays a critical role in any multi-sensor system and we achieve that using the “pulse per second (PPS)” technique. All the sensors sync to the CPU clock on the onboard computer, as can be seen in Figure 4. The IMU, LiDAR, and thermal camera directly use the CPU clock, whereas the 4 RGB cameras are synchronized using an FPGA board. Our experiments revealed that the time synchronization gap between any two sensors is not greater than 3ms.

3.3. IMU Calibration

We use the M-G365 inertial sensor¹ on our platform and calibrate it to reduce bias instability and drift. We employ an Allan variance[8] based tool² to estimate the white noise angle random walk and bias instability for both the gyroscope and accelerometer data. To this end, we collect a 1-hour IMU data sequence on a flat and stationary surface, consistent with other datasets like [28]. The same is made available in our dataset to the user. The IMU-LiDAR calibration is done using CAD models, the data for which will be made available to the user.

3.4. RGB Camera Calibration

We use an open-source calibration toolbox, Kalibr³ for the intrinsic and extrinsic calibration of the RGB camera. The camera is extrinsically calibrated to the IMU. For this purpose, we use a 7×9 checkerboard, the omnidirectional camera model, and the radial-tangential distortion model. A 60s random-motion video is used for the calibration, which will be provided to the user along with other parameters.

3.5. Thermal Camera Calibration

Calibrating a thermal camera follows a procedure similar to that of an RGB camera, with the addition of an image

processing task that requires obtaining a thermal calibration image with good contrast. This can be challenging, but we achieved it by heating a 7×9 chessboard under sunlight and feeding an inverted image from the recording into the Kalibr toolbox. Like the RGB camera, the thermal camera is also extrinsically calibrated to the IMU. This process uses a 60s random-motion clip, which we provide to the user along with other essential parameters.

3.6. Extrinsic Calibration for Multiple Robots

Collaborative tasks require multiple robots to operate in a common frame of reference. Our procedure to create this involves the usage of Generalized-ICP (GICP)[23] and is two-fold. In the first step, one robot shares its map from a feature-rich location to a base station. In the second step, the remaining robots take turns solving a GICP, in the same feature-rich location as the first robot and obtain a frame transformation from its own to the first robot. All the robots end up in a common frame after this procedure and build their map further using Super Odometry[29]. We will provide a graphic and mathematical description of this process in the supplemental material.

4. Dataset

Our dataset was recorded in the form of ROS bags, in diverse locations including rural and urban areas, and structured and unstructured sites, to provide varying levels of challenge for modern SLAM algorithms. The data contains multi-modal and sensor-degraded data and was recorded on multiple robots with varying kinematic profiles. The locations range from university campuses to caverns, buildings, and off-road areas (as shown in Figure 2). Here we briefly discuss our dataset in the following sub-sections. The detailed specifications of our dataset are further listed and discussed comprehensively in the supplementary material.

4.1. Multi Modal Dataset

Our dataset incorporates data from RGB cameras, thermal camera, LiDAR, and IMU, making it a multi-modal dataset. The majority of our dataset incorporates multi-modal data, recorded on different vehicles like the RC car, legged robot, and drones. This dataset has been collected in varied locations like caves, buildings, and university campus areas.

4.2. Multi Robot Dataset

Multi-robot SLAM(MR-SLAM) has garnered increasing attention in recent years due to its immense applications ranging from warehouse management, and autonomous truck fleets [13] to search and rescue [20].

To this end, a lot of focus is being put on building systems such as [5] to tackle the problem of MR-SLAM. This

¹https://global.epson.com/products_and_drivers/sensing_system/imu/g365/

²https://github.com/gaowenliang/imu_utils

³<https://github.com/ethz-asl/kalibr>

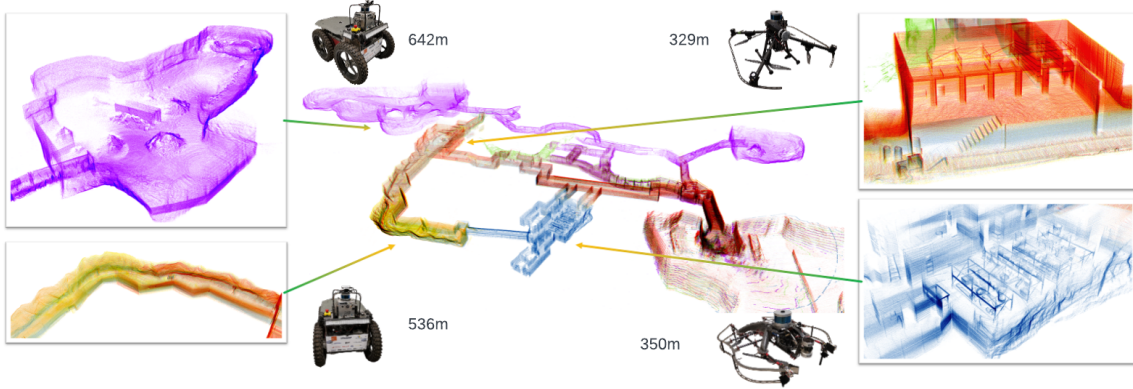


Figure 5: Point cloud of the Subt-MRS dataset, generated by Super Odometry[29]. Different colors represent point clouds collected by different robots.

naturally warrants a reliable multi-robot dataset, yet, as is visible from 1 none of the publicly available datasets provide detailed multi-robot data. To enable research and development of MR-SLAM systems, we are the first ones to provide **time** and **frame-synchronized sensor data** from 3 RC cars and a legged robot in a diverse environment. This data has been collected in the campus area, hospital building, and caves.

4.2.1 Synchronization

To get the best performance out of a multi-robot system, it is necessary to have all the robots operate in the same time and world frame. The time across all the robots is synchronized with respect to a common base station clock over Secure Shell. All the robots are aligned to the world frame using the calibration techniques explained in section 3.6.

4.3. Multi Degraded Dataset

Subt-MRS includes different sensor degradation categorized as visually degraded, geometrically degraded, and simultaneously degraded. In the following sections, we discuss the different types of sensor degradation in our dataset.

4.3.1 Visually Degraded

Visual degradation happens in areas with low visual textures like low-lit areas, smoke/fog, etc. In this dataset, we collect the data from subterranean and indoor environments, e.g., corridors.

- (a) **Low light and Darkness:** Our dataset includes several sequences in dim environments from the hospital building as well as the caves. The images A-F in Figure 2 provide a glimpse of the environment.

- (b) **Smoke and Dust:** Our dataset includes runs in smoke-filled areas in the hospital and caves. The images M-N in figure 2 show snapshots from these runs.

4.3.2 Geometrically Degraded

Geometric degradation relates to when environmental degradation of the LiDAR sensor either due to lack of structural features like planes, points, lines, etc, or due to LiDAR range deficit in big parking areas and long corridors leads to LiDAR odometry being unconstrained.

(a) Long corridor

In a featureless long corridor environment, the LiDAR range falls short. In this situation, the LiDAR sensor cannot constrain the estimation in the forward/backward direction. The image E from the hospital in Figure 2 shows an example of such environments.

(b) Stairs

LiDAR odometry tends to drift in staircases because of low feature access caused by fixed positioning of the LiDAR sensor on the platform, as shown in figure 3 and causes z-drift in LiDAR odometry. We have collected stair data on the university campus as well as the hospital. (Figure 2C,G)

4.3.3 Simultaneously Visually and Geometrically Degraded

Simultaneous visual and geometric degradation occurs if we combine the aforementioned scenarios. Such data can be useful for analyzing the robustness of multi-modal SLAM algorithms.

(a) **Dark corridor**

Long, dark corridors as shown in images A, E, and F of Figure 2 are a very general example of visual-geometric degradation.

(b) **Dark stairs**

As shown in image C of Figure 2, we have runs of the legged robot on dark staircases with the LED lights turned on.

(c) **Snowy stairs**

Data was also collected in snowy environments, as can be seen in images H, K, and L of Figure 2. Snow leads to visual degradation due to loss of RGB texture because of white-capped environments. Additionally, snowflakes can show up as spoof point features for LiDAR odometry, leading to drift.

5. Ground Truth Map

5.1. Instruments

In our approach to creating a ground truth map, we utilize a combination of surveying techniques and advanced measurement tools. Specifically, the Leica Viva Total Station 15A is used to provide accurate distance and angle measurements. The Leica Mini 360 Prism is utilized to reflect the laser back to the Total Station with high precision, and the robotic aiming feature is employed to ensure consistency and reliability in unlit hallways and interior spaces. Additionally, we use the FARO Focus 3D S120 for precise dense point cloud measurements, with its high accuracy obtained through a laser ranger. Finally, checkerboard fiducial targets are used in select areas to supplement the software used for matching and alignment.

5.2. Data Collection

This study performs Ground Truth modeling at two locations in Pittsburgh, PA, USA: an abandoned hospital and Carnegie Mellon University campus. The hospital survey utilizes a Total Station survey instrument with eye bolts installed at strategic locations to measure points around a large loop. With the loop closure algorithm, an error of approximately 3.4 cm is yielded, and the model covers an area of roughly 350 meters by 350 meters, including several buildings and surrounding landscapes. On the other hand, the Carnegie Mellon University campus survey focuses on four buildings near the Newell-Simon Hall and utilizes 79 FARO scans to generate a model with an expected accuracy of less than 2cm. The survey covers an area of about 200 meters by 200 meters and results in a highly accurate model. The dataset generated from these surveys exceeds 750Gb of data, providing valuable resources for various research and applications. The ground truth maps for all the datasets will

be provided to the users. A glimpse of these ground truth maps is provided in the supplementary material.

5.3. Ground Truth Trajectory

5.3.1 Generation

Ground truth trajectories are generated for all datasets, using Super Odometry [29] with a modified Laser Odometry algorithm. As shown in Figure 6, the ground truth point cloud is pre-processed using a feature extraction module that assesses “local linearity, planarity, and curvatures of geometric feature” [29], with the extracted geometric features stored. As new LiDAR scans arrive, a subset of the ground truth points is selected from the stored features based on the current pose and used as the reference for Iterative Closest Point (ICP). The resulting ICP output is integrated into the normal Super Odometry procedures. Visual Odometry is employed to help constrain pose estimation in datasets with degraded geometry, such as long corridor environments.

5.3.2 Evaluation

In this study, we assess the accuracy of the created trajectories by employing Map Analysis⁴, an open-source tool that calculates the map deviation utilizing both the integrated point cloud and the ground truth map. The modified ground truth trajectories provide both the trajectory and the integrated point cloud. To quantify the map deviation, we introduce the distance metric d_i^j , defined as the euclidean distance between point i and its corresponding point j in the ground truth map. We then identify the set of outlier points using the deviation threshold of 1.0m specified in Equation 1.

$$\text{Outlier Points} : d_i^j > 1.0m \quad (1)$$

The map deviation is computed by dividing the number of outlier points by the total number of points, as shown in Equation 2.

$$\sigma = \frac{N_{\text{Outlier Points}}}{N_{\text{Total Points}}} \quad (2)$$

To ensure the validity of the generated ground truth trajectory, we require that the map deviation of its integrated point cloud is less than 1%. This threshold value accounts for the possibility that some LiDAR scan points may not be covered by the ground truth map. Notably, we observe that all the identified outliers originate from rooms that lie outside the coverage area of the ground truth map for the long corridor. After excluding the points in the rooms outside the coverage area of the ground truth map for the long corridor, our trajectory generation result achieved a map deviation of less than 0.1%.

⁴https://github.com/subtchallenge/map_analysis

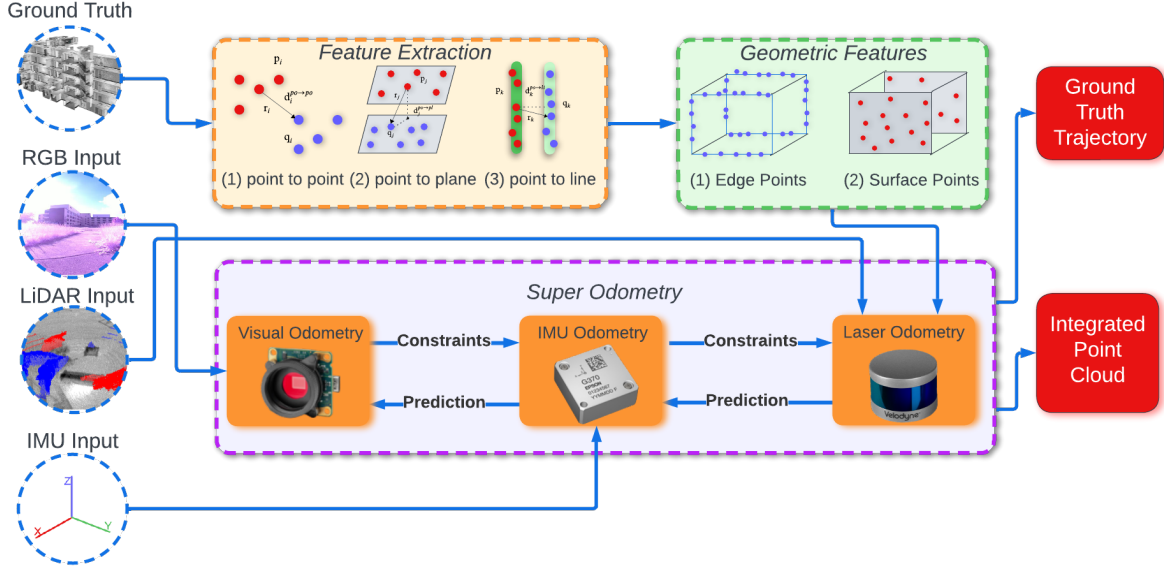


Figure 6: Overview of ground truth trajectories generation on modified Super Odometry. Ground truth geometric features are extracted and stored in the pre-processing phase. Laser Odometry is modified to use stored ground truth features to provide accurate constraints. The ground truth trajectory is formed by collecting ground truth poses estimated by Super Odometry.

Runs in Subt-MRS			SLAM Algorithms' Map Deviation (%)					
Robot	Run Length (m)	Run Time(s)	Fast_LIO[26]	Faster_LIO[1]	LIO_SAM[24]	Clins[15]	ALOAM[27]	Super Odometry[29]
Canary	329	591.3	≥ 50	31.43	≥ 50	16.01	37.91	0.09
DS3	350.6	607.42	0.03	0.08	≥ 50	1.39	0.01	0.006
DS4	238	484.7	13.78	12.48	≥ 50	3.43	10.72	0.15
R1	436.4	600	28.99	34.91	≥ 50	16.4	32.95	0.07
R2	536	1909	4.36	10.42	≥ 50	16.05	7.6	0.07
R3	642	1713	≥ 50	≥ 50	≥ 50	≥ 50	40.8	2.4

Table 3: Map Deviation of different SLAM algorithms running on Subt-MRS datasets

6. Challenging Results and Findings

6.1. Results

The Subt-MRS dataset provides a comprehensive framework for evaluating the performance of different SLAM algorithms. To analyze the limitations of current state-of-the-art SLAM methods, we conduct extensive evaluations on various LiDAR-only, LiDAR-Inertial, and LiDAR-Visual-Inertial SLAM algorithms using our dataset. To ensure diversity in our analysis, we select three runs collected by drones (Canary, DS3, DS4) and three runs collected by ground robots (R1, R2, R3) in a distinct section of the subterranean environment. In our evaluations, we focus on the LiDAR data from R3, which has a higher level of sensor noise and collect sequences to assess the algorithms' robustness under such disturbances. To quantify the performance of each algorithm, we compare the reconstructed maps against the ground truth map and estimate the map deviations. Our results are presented in Table 3, and the point cloud data used in our evaluations are shown in Figure 5.

6.2. Discussion

The evaluation results in Table 3 provide insights into the performance of various SLAM algorithms on the Subt-MRS dataset. Super Odometry stands out as the most robust algorithm, achieving an average deviation of only 0.5%. The combination of LiDAR, visual camera, and IMU sensors in Super Odometry provides greater resilience against challenging environmental conditions. In contrast, LiDAR-Inertial and LiDAR-Only algorithms, such as Fast_LIO, Faster_LIO, and ALOAM, show significant drift in most runs, indicating limited robustness in multi-degraded environments. Clins, which implements continuous-time trajectory estimation, performs better than other LiDAR-Inertial and LiDAR-Only algorithms, with deviations of less than 17% in most runs. However, Clins operates offline, which may not be suitable for real-time applications. The results suggest that the use of additional sensors and advanced estimation techniques is necessary to achieve high robustness in challenging environments.

References

- [1] Chungge Bai, Tao Xiao, Yajie Chen, Haoqian Wang, Fang Zhang, and Xiang Gao. Faster-lio: Lightweight tightly coupled lidar-inertial odometry using parallel sparse incremental voxels. *IEEE Robotics and Automation Letters*, 7(2):4861–4868, 2022.
- [2] Michael Burri, Janosch Nikolic, Pascal Gohl, Thomas Schneider, Joern Rehder, Sammy Omari, Markus W Achtelik, and Roland Siegwart. The EuRoC micro aerial vehicle datasets. *The International Journal of Robotics Research*, 2016.
- [3] Carlos Campos, Richard Elvira, Juan J. Gómez Rodríguez, José M. M. Montiel, and Juan D. Tardós. Orb-slam3: An accurate open-source library for visual, visual-inertial, and multimap slam. *IEEE Transactions on Robotics*, 37(6):1874–1890, 2021.
- [4] Nicholas Carlevaris-Bianco, Arash K Ushani, and Ryan M Eustice. University of michigan north campus long-term vision and lidar dataset. *The International Journal of Robotics Research*, 35(9):1023–1035, 2016.
- [5] Yun Chang, Kamak Ebadi, Christopher E. Denniston, Muhammad Fadhil Ginting, Antoni Rosinol, Andrzej Reinke, Matteo Palieri, Jingnan Shi, Arghya Chatterjee, Benjamin Morrell, Ali-akbar Agha-mohammadi, and Luca Carlone. Lamp 2.0: A robust multi-robot slam system for operation in challenging large-scale underground environments, 2022.
- [6] Jeffrey Delmerico, Titus Cieslewski, Henri Rebecq, Matthias Faessler, and Davide Scaramuzza. Are we ready for autonomous drone racing? the UZH-FPV drone racing dataset. In *IEEE Int. Conf. Robot. Autom. (ICRA)*, 2019.
- [7] Rodolphe Dubois, Alexandre Eudes, and Vincent Frémont. Airmuseum: a heterogeneous multi-robot dataset for stereo-visual and inertial simultaneous localization and mapping. In *2020 IEEE International Conference on Multisensor Fusion and Integration for Intelligent Systems (MFI)*, pages 166–172, 2020.
- [8] Naser El-Sheimy, Haiying Hou, and Xiaoji Niu. Analysis and modeling of inertial sensors using allan variance. *IEEE Transactions on Instrumentation and Measurement*, 57(1):140–149, 2008.
- [9] Adrien Gaidon, Qiao Wang, Yohann Cabon, and Eleonora Vig. Virtual worlds as proxy for multi-object tracking analysis. In *Proceedings of the IEEE conference on computer vision and pattern recognition*, pages 4340–4349, 2016.
- [10] Andreas Geiger, Philip Lenz, Christoph Stiller, and Raquel Urtasun. Vision meets robotics: The kitti dataset. *The International Journal of Robotics Research*, 32(11):1231–1237, 2013.
- [11] Andreas Geiger, Philip Lenz, and Raquel Urtasun. Are we ready for autonomous driving? The KITTI Vision Benchmark Suite. In *Conference on Computer Vision and Pattern Recognition (CVPR)*, 2012.
- [12] Michael Helmberger, Kristian Morin, Beda Berner, Nitish Kumar, Giovanni Cioffi, and Davide Scaramuzza. The hilti slam challenge dataset. *IEEE Robotics and Automation Letters*, 7(3):7518–7525, 2022.
- [13] P. Y. Lajoie, B. Ramtoula, F. Wu, and G. Beltrame. Towards collaborative simultaneous localization and mapping: A survey of the current research landscape. *Field Robotics*, 2:971–1000, 2022.
- [14] Keith YK Leung, Yoni Halpern, Timothy D Barfoot, and Hugh HT Liu. The utias multi-robot cooperative localization and mapping dataset. *The International Journal of Robotics Research*, 30(8):969–974, 2011.
- [15] Jiajun Lv, Kewei Hu, Jinhong Xu, Yong Liu, Xiushui Ma, and Xingxing Zuo. CLINS: continuous-time trajectory estimation for lidar-inertial system. *CoRR*, abs/2109.04687, 2021.
- [16] Will Maddern, Geoffrey Pascoe, Chris Linegar, and Paul Newman. 1 year, 1000 km: The oxford robotcar dataset. *The International Journal of Robotics Research*, 36(1):3–15, 2017.
- [17] Bernd Pfrommer, Nitin Sanket, Kostas Daniilidis, and Jonas Cleveland. PenncoSyvio: A challenging visual inertial odometry benchmark. In *2017 IEEE International Conference on Robotics and Automation (ICRA)*, pages 3847–3854. IEEE, 2017.
- [18] Taihú Pire, Martín Mujica, Javier Civera, and Ernesto Kofman. The rosario dataset: Multisensor data for localization and mapping in agricultural environments. *The International Journal of Robotics Research*, 38(6):633–641, 2019.
- [19] Tong Qin, Peiliang Li, and Shaojie Shen. Vins-mono: A robust and versatile monocular visual-inertial state estimator. *IEEE Transactions on Robotics*, 34(4):1004–1020, 2018.
- [20] Jorge Peña Queralta, Jussi Taipalmaa, Bilge Can Pullinen, Victor Kathan Sarker, Tuan Nguyen Gia, Hannu Tenhunen, Moncef Gabbouj, Jenni Raitoharju, and Tomi Westerlund. Collaborative multi-robot search and rescue: Planning, coordination, perception, and active vision. *IEEE Access*, 8:191617–191643, 2020.
- [21] Milad Ramezani, Yiduo Wang, Marco Camurri, David Wisth, Matias Mattamala, and Maurice Fallon. The newer college dataset: Handheld lidar, inertial and vision with ground truth. In *2020 IEEE/RSJ International Conference on Intelligent Robots and Systems (IROS)*, pages 4353–4360. IEEE, 2020.
- [22] David Schubert, Thore Goll, Nikolaus Demmel, Vladyslav Usenko, Jörg Stückler, and Daniel Cremers. The tum vi benchmark for evaluating visual-inertial odometry. In *2018 IEEE/RSJ International Conference on Intelligent Robots and Systems (IROS)*, pages 1680–1687. IEEE, 2018.
- [23] Aleksandr Segal, Dirk Haehnel, and Sebastian Thrun. Generalized-icp. In *Robotics: science and systems*, volume 2, page 435. Seattle, WA, 2009.
- [24] Tixiao Shan, Brendan Englot, Drew Meyers, Wei Wang, Carlo Ratti, and Rus Daniela. Lio-sam: Tightly-coupled lidar inertial odometry via smoothing and mapping. In *IEEE/RSJ International Conference on Intelligent Robots and Systems (IROS)*, pages 5135–5142. IEEE, 2020.
- [25] Wenshan Wang, Delong Zhu, Xiangwei Wang, Yaoyu Hu, Yuheng Qiu, Chen Wang, Yafei Hu, Ashish Kapoor, and Sebastian Scherer. Tartanair: A dataset to push the limits of visual SLAM. In *2020 IEEE/RSJ International Conference on Intelligent Robots and Systems (IROS)*, 2020.
- [26] Wei Xu, Yixi Cai, Dongjiao He, Jiarong Lin, and Fu Zhang. FAST-LIO2: fast direct lidar-inertial odometry. *IEEE Trans-*

actions on Robotics, abs/2107.06829, 2022.

- [27] Ji Zhang and Sanjiv Singh. Loam : Lidar odometry and mapping in real-time. *Robotics: Science and Systems Conference (RSS)*, pages 109–111, 01 2014.
- [28] Lintong Zhang, Marco Camurri, and Maurice Fallon. Multi-camera lidar inertial extension to the newer college dataset. *arXiv preprint arXiv:2112.08854*, 2021.
- [29] Shibo Zhao, Hengrui Zhang, Peng Wang, Lucas Nogueira, and Sebastian Scherer. Super odometry: Imu-centric lidar-visual-inertial estimator for challenging environments. In *2021 IEEE/RSJ International Conference on Intelligent Robots and Systems (IROS)*, pages 8729–8736. IEEE, 2021.
- [30] David Zuñiga-Noël, Alberto Jaenal, Ruben Gomez-Ojeda, and Javier Gonzalez-Jimenez. The uma-vi dataset: Visual-inertial odometry in low-textured and dynamic illumination environments. *The International Journal of Robotics Research*, 39(9):1052–1060, 2020.